ACS OMEGA

http://pubs.acs.org/journal/acsodf

Article

Occurrence Modes of Critical Metals (Li^+ and Ge^{4+}) in the Organic Molecular Structures of Coal: A Density Functional Theory Study

Ruifeng Mu, Shaoqing Wang,* Xiaoling Wang, Yungang Zhao, and Zeyu Dong

Cite This: *ACS Omega* 2023, 8, 17264−17273

Read Online

ACCESS | Metrics & More | Article Recommendations | Supporting Information

ABSTRACT: To explore the mechanism of critical metal (Li^+ and Ge^{4+}) occurrence in the organic molecular structures of different rank coals, simulations were investigated using quantum chemical density functional theory. In this paper, Wender lignite, bituminous, and anthracite molecular models were used as organic molecular structures in coal. The electrostatic potential (ESP), frontier molecular orbitals, and Mulliken charges were used to identify adsorption sites in organic molecular structures. Mulliken charge, bond length, Mayer bond order (MBO), and adsorption energy values were used to estimate the binding conformation and strength between organic molecular structures and critical metals (Li^+ and Ge^{4+}). The results showed that the negative ESP, the highest occupied molecular orbitals, and negative Mulliken charges in the organic molecular structures were located at the O atom of oxygen functional groups and the aromatic structures, respectively, which were the active sites for critical metal adsorption. Mulliken charge transfer, bond length, MBO, and adsorption energy data suggested that the binding of Li^+ with organic molecular structures was controlled by the carbonyl group (C═O), while the aromatic structures had less effect on the occurrence of Li^+ in the organic molecular structures. The maximum adsorption energy value for binding Li^+ with organic molecular structures was −742.16 kJ/mol. The Ge^{4+} ions not only showed strong binding ability with oxygen functional groups, but also Ge^{4+} formed thermodynamically stable half-sandwich complexes with aromatic structures. Therefore, the coal rank had little effect on the binding of Ge^{4+} with organic molecular structures. Moreover, the binding of Ge^{4+} with organic molecule structures was enhanced by the synergistic interactions of oxygen functional groups and aromatic structures. The adsorption energy values were up to −8511.43 kJ/mol. The adsorption of organic matter in coal to critical metals (Li^+ and Ge^{4+}) generated changes in the spatial configuration of the organic molecular structure, including local twisting of the organic molecular structure in lignite and bending of the aromatic structure in anthracite.

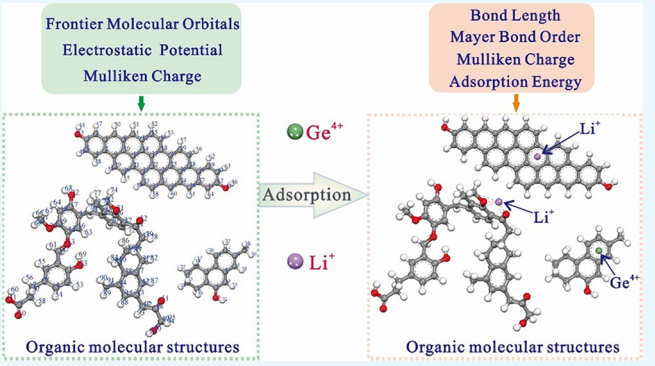

1. INTRODUCTION

Critical metals, such as lithium (Li) and germanium (Ge), are essential to national life and defense security. They have already been utilized in batteries, biomedicine, and the nuclear industry. Their primary source is conventional ore deposits. However, conventional ore deposits are becoming increasingly scarce and expensive, resulting in a growing gap between supply and demand.[1] In recent years, most scholars have discovered that critical metals are enriched in coal and coal combustion products (CCPs), e.g., Li, Ge, Ga, and REEs.[2−6] Their concentrations reach the extent and grades required for industrial use.[6−9] In particular, concentrations of Li_2O are up to 0.72−0.83% in the ashes of Li-rich coal benches.[10] The percentage of Ge in fly ash from Ge-rich coal combustion can be up to 5%.[11] Therefore, coal-hosted rare-metal deposits have enormous potential for critical metal extraction. Nonetheless, the occurrence modes of critical metals closely related to the organic matter in coal are still emerging.

Critical metals in coal may be related to inorganic and organic fractions, and organic matter is essential in mineralizing coal-based strategic metallic minerals.[12] The macromolecular structure of coal organic matter is mainly an aromatic structure with alkyl side chains, various oxygen functional groups, and bridge bonds attached around it. Unfortunately, detailed information on the interactions between critical metals and organic matter in coal is scanty.[13] The affinity of Li with organic matter in coal was usually obtained by indirect methods such as concentration distribution functions,[14] correlation analysis,[15,16] and selective leaching experiments.[17] Nevertheless, the exact organic location of Li is still unclear. On the contrary, Ge is the only element almost 100% organically associated with coal.[18,19] This was demonstrated by direct and indirect methods such as

Received: March 16, 2023
Accepted: April 18, 2023
Published: May 5, 2023

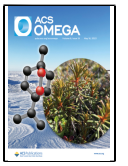

https://doi.org/10.1021/acsomega.3c01801
ACS Omega 2023, 8, 17264−17273

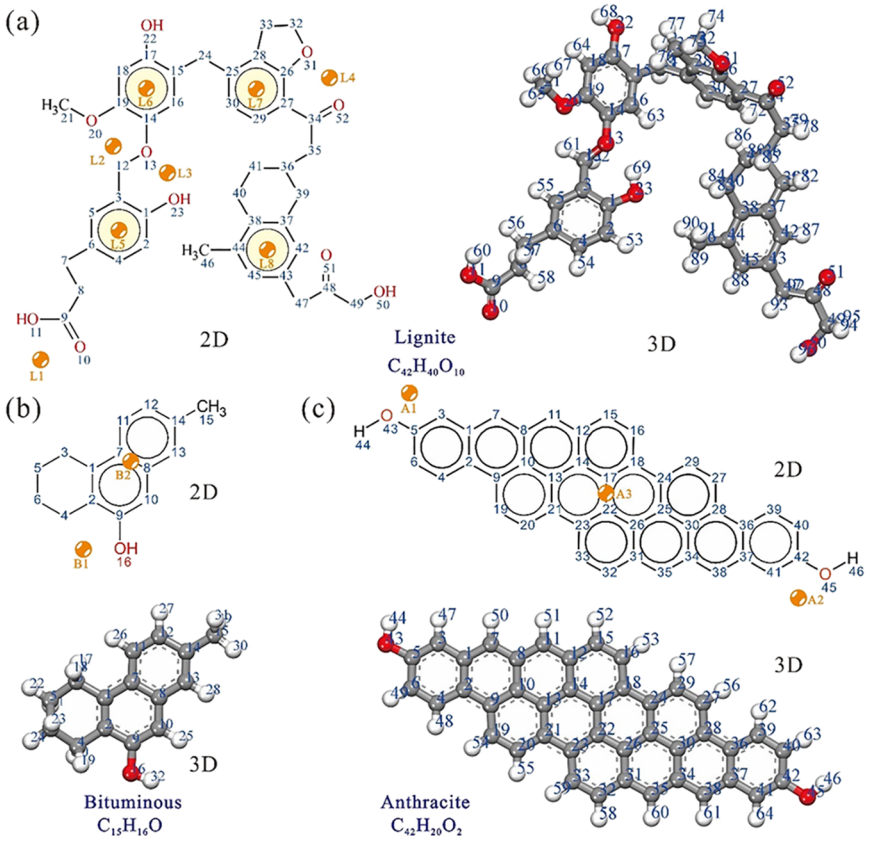

Figure 1. 2D and 3D molecular models of organic molecular structures. C, H, and O atoms are shown as gray, white, and red, respectively (similarly hereinafter). Orange represents different adsorption sites. Organic molecular structure of (a) lignite, (b) bituminous, (c) anthracite [Adapted in part with permission from ref 40. Copyright 1976, Catalysis Reviews-Science and Engineering].

correlation analysis and spectrum analysis.[20−23] Furthermore, the spectrum analysis result shows that Ge in coal exists in a tetravalent oxidation state and deformed octahedral coordination with oxygen. The Ge in coal exists in the form of chelation with organic matter,[2,24,25] among which carboxyl, catechols, and hydroxyl groups are the primary binding sites.[26−28] Although some oxygen functional groups have been postulated to bind to critical metals, direct evidence is insufficient and difficult to obtain.[13] Furthermore, the role of aromatic structures, i.e., π-cation interactions, is also ignored.

The π-cation interaction is considered one of the noncovalent binding forces.[29,30] The interactions of Li^+ and Na^+ with aromatic structures (π-cation interactions) in coal have been analyzed by Fourier transform infrared spectroscopy (FTIR).[31] The microscopic mechanism of aromatic structures binding to critical metals, however, has not been reported further in the literature. Fortunately, density functional theory (DFT) can quantify the microscopic adsorption mechanism of organic matter binding to critical metals in coal. This method has been applied to investigate the interaction of metal ions (K^+, Li^+, Y^{3+}, and Sr^{2+}) with minerals or organic matter (humic acid and lignin).[32−35] Mixed functional groups are thought to stabilize metal complexes when critical metals bind to organic matter.[32,33,36] Furthermore, critical metals have an impact on the stability of organic matter, such as the observed catalytic effect of Li^+ and Be^{2+} in the lignin molecular structure, leading to the elongation of C_β−O. At the same time, Mg^{2+} makes the structure more stable.[37,38] DFT calculations allow us to understand how critical metals interact with organic matter in coal on the molecular level. Although this form of interaction cannot be completely accurate, qualitative information about the interaction energies of organic matter in coal and critical metals can be obtained. Previous research only used small molecular fragments or humic acids to represent coal's molecular structure. If a suitable coal molecular structure can be selected, the interactions of critical metals with organic matter in coal can be identified. In this case, the occurrence modes of critical metals in organic matter can be clearly understood.

Identifying the occurrence modes of critical metals in the organic matter of coal can help improve the procedure for extracting critical metals from coal and CCPs, as well as reduce hazardous releases of critical metals to the environment during utilization.[8,39] In this paper, in addition to analyzing the microscopic mechanisms of critical metals' occurrence modes in organic molecular structures, the binding of organic molecular structures with critical metals in different rank coals is also considered. This is because as the coal rank increases, the oxygen functional groups (−COOH and $-OCH_3$) in coal gradually decrease or even disappear, while the proportion of aromatic structures gradually increases. Therefore, it is necessary to consider the effect of changes in the coal structure on the binding of organic molecular structures with critical metals (Li^+ and Ge^{4+}) in coal. The binding sites in the organic molecular structures of different rank coals are determined using the electrostatic potential (ESP), frontier molecular orbital (FMO), and Mulliken charges. The binding conformation, binding ability, and optimal binding sites of organic molecular structures with critical metals (Li^+ and Ge^{4+}) in different rank coals are determined using the Mulliken charge, bond length, Mayer bond order (MBO), and adsorption energy. The occurrence of critical

https://doi.org/10.1021/acsomega.3c01801
ACS Omega 2023, 8, 17264−17273

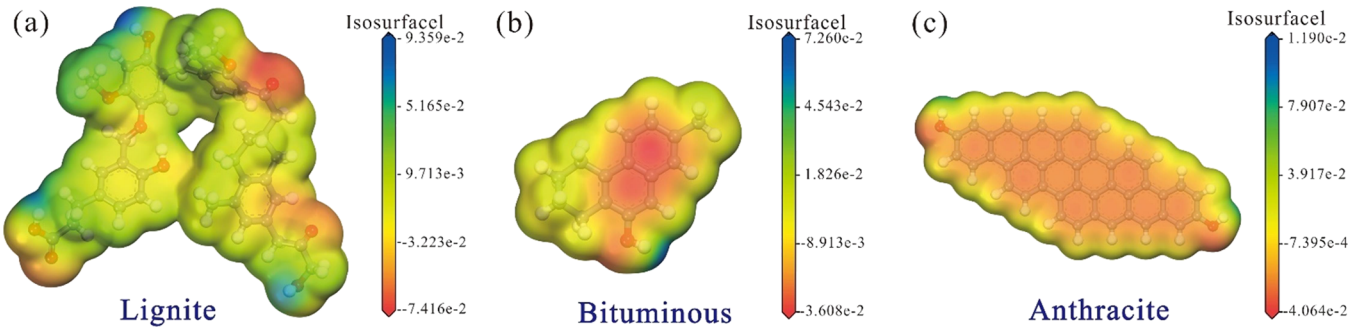

Figure 2. ESP of organic molecular structures. Red represents regions of the most negative ESP, blue represents the most positive ESP, and yellow represents regions of zero potential. Organic molecular structures of (a) lignite, (b) bituminous, and (c) anthracite.

metals (Li^+ and Ge^{4+}) in the organic molecular structure of coal was analyzed to gain a deeper understanding at the molecular level.

2. THEORETICAL METHODS

2.1. Selection of Organic Molecular Structures in Coal. Wender lignite, bituminous, and anthracite molecular models were used in this study to investigate the adsorption characteristics of organic molecular structures with critical metals. The linkage sites were saturated with hydrogen. The molecular formulas of the models were $C_{42}H_{40}O_{10}$, $C_{15}H_{16}O$, and $C_{42}H_{20}O_2$, respectively.[40] The organic molecular structure of lignite includes a benzene ring, an ordinary six-carbon ring, oxygen functional groups, and aliphatic side chains. It has been widely applied to the study of coal pyrolysis/gasification,[41] interfacial water,[42] mechanochemistry,[43,44] and wettability.[45] The carboxyl and methoxy groups decrease dramatically as the coal rank rises.[46,47] This process enhances the effect of ring condensation and generates larger aromatic structural units. Wender coal models are well indicators of this metamorphic process. The Wender coal models lacked functional groups containing N and S atoms. Therefore, interactions between N- and S-containing functional groups and organic molecular structures are excluded. The 2D and 3D molecule models of the organic molecular structures in Wender lignite, bituminous, and anthracite were sketched by ACD/ChemSketch and Materials Studio software (Accelrys Inc.), respectively (Figure 1).

2.2. Calculation Details. The calculations of ESP, FMO, Mulliken charge, bond length, MBO, and adsorption energy were performed by the DMol^3 module in Materials Studio software, which has been widely used to study the binding mechanism between metal atoms/ions or small molecules and nanostructures.[48,49] The electronic exchange-correlation energy was treated within the generalized gradient correction (GGA) of the Perdew−Burke−Ernzerhof (PBE) functional.[50] Considering the solvation effect, the conductor-like shield model (COSMO) with a permittivity of 78.54 (water) was selected. All electron (AE) methods were used for core processing. The dual numerical polarization method (DNP 4.4) was used to describe the electronic basis set, and the Grimme method was used for DFT-D correction.[51] AE calculations were performed with unrestricted electron spin.[52] The accuracy was set at "Fine". The electron self-consistent field (SCF) convergence value was 1.0×10^{-6} Ha. The convergence tolerance values for energy, maximum force, and maximum displacement were 1×10^{-5} Ha, 2×10^{-3} Ha/Å, and 5×10^{-3} Å, respectively. The DMol^3 module performed the geometry optimization of all organic molecular structures. Adsorption energy analysis was performed to determine the binding capacity of organic molecular structures in coal with critical metals. The adsorption energy of different adsorption sites in organic molecular structures with critical metals was calculated as follows:

$$\Delta E_{ads} = E_{coal-ions} - (E_{coal} + E_{ions}) \quad (1)$$

where $E_{coal-ions}$ is the total energy for the adsorption complex, E_{coal} is the total energy of the adsorbent, and E_{ions} is the total energy of the adsorbate. The absolute value of adsorption energy is positively correlated with adsorption capacity.

2.3. Selection of Adsorption Sites. ESP, FMO, and Mulliken charge evaluated adsorption sites of organic molecular structures. The electronegative region on the surface of organic molecular structures exhibited a strong adsorption capacity for critical metals. The molecular orbital theory was also crucial to analyze the chemical reactions of molecular systems because electrons in front orbitals were usually more active.[53] It was simple to cause electron transfer, bond formation, or bond breakage, leading to a reaction.[54] The atoms with the highest negative Mulliken charge in organic molecular structures coordinated best with the critical metals.[55] In addition, the previous literature on binding organic matter (small molecular fragments or humic acids) with metal ions was referred to.[32,33] Accordingly, we selected the oxygen functional groups and the aromatic structures in organic molecular structures as the binding sites for Li^+ and Ge^{4+}. As shown in Figure 1, the organic molecular structure adsorption sites in lignite were O10−O11 (L1), O13−O20 (L2), O13−O23 (L3), O31−O52 (L4), and four benzene ring positions (L5, L6, L7, and L8). Organic molecular structures with adsorption sites in bituminous were O16 (B1) and C7−C8 centers (B2). Organic molecular structures with adsorption sites in anthracite were O43 (A1), O45 (A2), and C17−C22 centers (A3). The selection of adsorption sites for organic molecular structures in coal and the binding strength of different adsorption sites with critical metals will be described in more detail below.

3. RESULTS AND DISCUSSION

3.1. ESP Analysis. The positive and negative ESP of the molecular regions can be localized by ESP analysis, providing a visual understanding of the relative polarity of the molecules. The different values of ESP on the surface of the organic molecular structures were indicated by several colors. The potential increases in the order red < orange < yellow < green < blue.[56] As shown in Figure 2, lignite's organic molecular structure contained multiple oxygen functional groups and a wide range of negative potentials. The negative potentials were mainly concentrated on the carboxyl (O10 and O11) and

https://doi.org/10.1021/acsomega.3c01801
ACS Omega 2023, 8, 17264−17273

carbonyl (O51 and O52) groups, indicating that they are prone to electrophilic reactions. However, many aliphatic side chains in lignite's organic molecular structure resulted in a near-neutral ESP of the aromatic structures. The maximum negative potential of the organic molecular structure in lignite was 7.416×10^{-2} au, while the maximum positive potential was 9.359×10^{-2} au near the hydrogen atoms. In contrast, the bituminous and anthracite organic molecular structures contained fewer oxygen functional groups, resulting in a more uniform distribution of ESP. The negative potentials were mainly concentrated on the aromatic structures and the O atoms (O16, O43, and O45) of the hydroxyl group. The hydrogen atoms on the phenols showed positive potentials, indicating that they are prone to nucleophilic reactions, while the other regions were electrically neutral. The maximum negative potentials were 3.608×10^{-2} and 4.064×10^{-2} au for the organic molecular structures in bituminous and anthracite, respectively, and the maximum positive potentials were 7.260×10^{-2} and 1.190×10^{-2} au, respectively. The results showed that the oxygen functional groups and aromatic structures were the main adsorption sites for critical metals (Li^+ and Ge^{4+}).

3.2. FMO Analysis. The highest occupied molecular orbital (HOMO) and the lowest unoccupied molecular orbital (LUMO) are crucial to determining the reaction site of a molecular structure.[57] The HOMO and the nearby occupied orbitals are essential in supplying electrons preferentially. In contrast, the LUMO and the nearby vacant orbitals are essential for accepting electrons. The HOMO representations of organic molecular structures are shown in Figure 3. We considered only HOMOs because the organic molecular structures acted as electron donors in this study, transferring their electrons from HOMOs to the orbitals of the critical metals. As shown in Figure 3, the HOMOs in the organic molecular structure of lignite were mainly confined to the carbonyl group (O52) and ether oxygen (O31) positions, indicating that this was the chelating part of the critical metals. HOMOs were mainly concentrated on aromatic structures and the O16 atom of the hydroxyl group in the organic molecular structures of bituminous. HOMOs were concentrated on aromatic structures in the organic molecular structures of anthracite, exhibiting the π characteristic. This was almost the same result as that observed by the ESP.

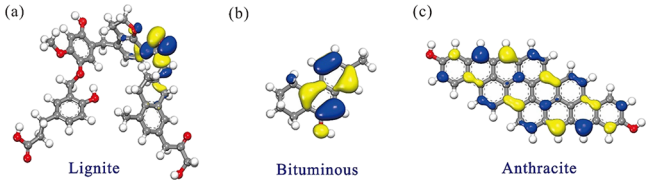

Figure 3. HOMO of organic molecular structures. Blue represents the positive phase, and yellow represents the negative phase. Organic molecular structures of (a) lignite, (b) bituminous, and (c) anthracite.

3.3. Mulliken Charge Analysis. The charge distribution and transfer can be calculated using Mulliken charge analysis.[58] The exact values are shown in Table S1. The oxygen atoms were all high in electronegativity. Mulliken charge transfer values are positively correlated with the strength of the interactions. The critical metals always gain electrons when bound with the oxygen functional groups and aromatic structures. Still, the oxygen atoms and phenyl carbon almost lost electrons after the reaction, indicating the existence of donor−acceptor interactions in these complexes. In the organic molecular structures of lignite, the maximum and minimum changes of charge transfer for the binding of Li^+ with oxygen functional groups were located at the L4 and L1 adsorption sites, with values of 0.196 e and 0.122 e, respectively. The maximum charge transfer of Li^+ bonded with the aromatic structure occurred at the L7 adsorption site, with a value of 0.195 e, which was almost the same as the value of the L4 adsorption site. It showed that Li^+ binds optimally with organic molecular structures at the L4 adsorption site. This was the same as the binding site indicated by the ESP and HOMOs. In the organic molecular structures of bituminous and anthracite, the charge transfer values between Li^+ and oxygen functional groups were slightly higher than those of aromatic structures. Therefore, Li^+ was marginally preferred to bind oxygen functional groups in organic molecular structures. Furthermore, it was found that the electron transfer between Li^+ and either the oxygen functional groups or the aromatic structures decreased as the coal rank increased (Figure 4a). This demonstrates that as the coal rank increased, the binding capacity of Li^+ with organic molecular structures decreased.

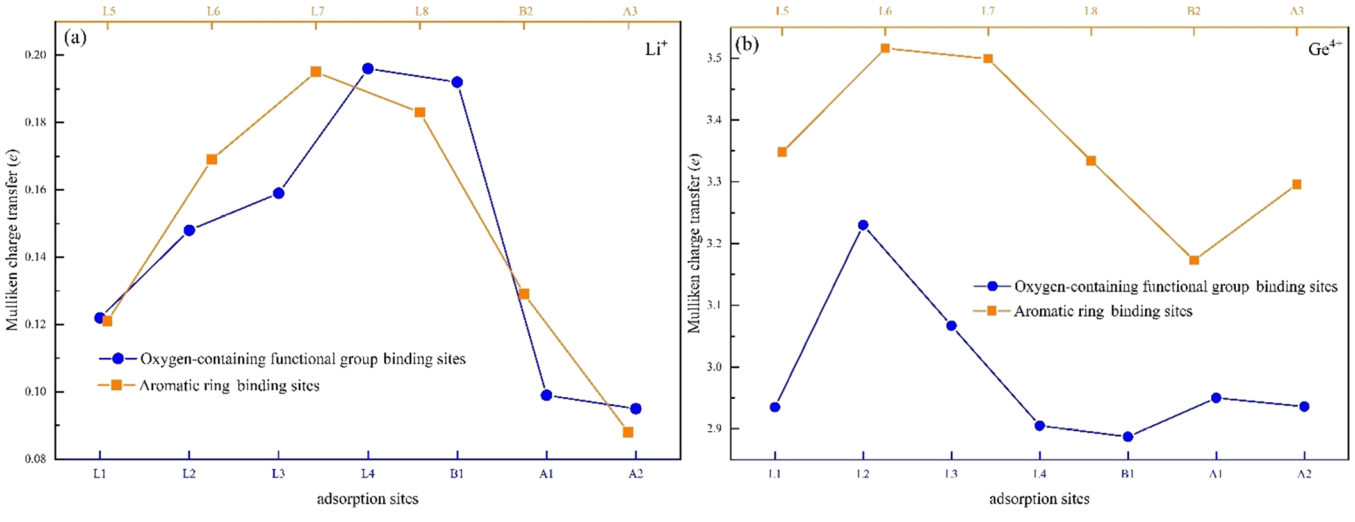

Figure 4. Charge transfer values between critical metals and organic molecular structures. (a) Li^+. (b) Ge^{4+}.

https://doi.org/10.1021/acsomega.3c01801
ACS Omega 2023, 8, 17264−17273

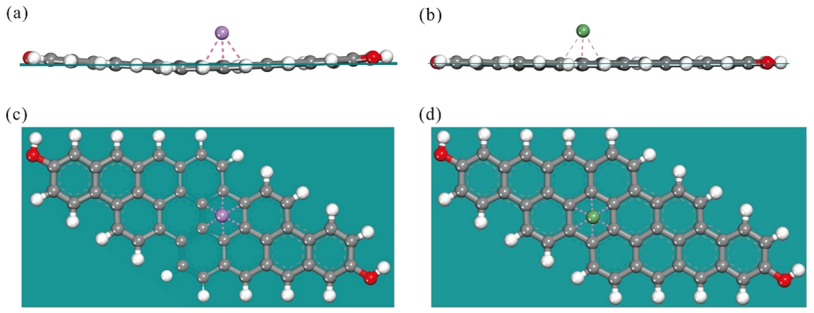

Figure 5. Bending deformation of the organic molecular structure in anthracite. Li^+ and Ge^{4+} are shown as purple and green, respectively (similarly hereinafter). Cyan represents the isosurface. (a, b) Side view of the organic molecular structure and critical metal configuration. (c, d) Top view of the organic molecular structure and critical metal configuration.

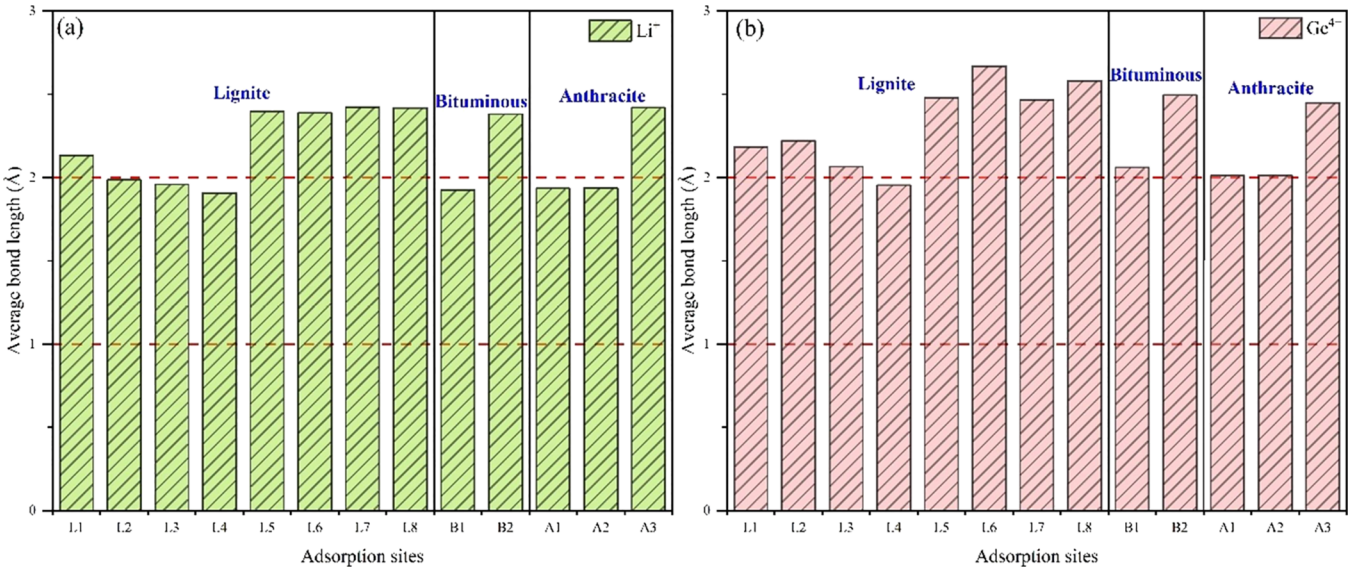

Figure 6. Average bond length values between critical metals and organic molecular structures. (a) Li^+. (b) Ge^{4+}.

The charge of metal ions is positively correlated with the electron transfer capacity.[59] Therefore, the charge transferred between Ge^{4+} and oxygen functional groups and aromatic structures was much higher than that between Li^+. In the organic molecular structures of lignite, the maximum charge transfer of Ge^{4+} bound with oxygen functional groups was at the L2 adsorption site, followed by the L3 adsorption site, with values of 3.230 e and 3.067 e, respectively. The charge transfer between Ge^{4+} and the aromatic structures was more significant than that between Ge^{4+} and the oxygen-containing functional group (Figure 4b). For example, the Mulliken charges of Ge^{4+} at the L6 and L7 adsorption sites were as high as 3.516 e and 3.499 e, respectively. This trend also existed in the organic molecular structures of bituminous and anthracite. Therefore, the aromatic structures in organic molecular structures played an essential role in the occurrence of Ge^{4+}. Li^+ and Ge^{4+} were oriented exactly above the centers of the six-membered rings. The electronic contribution of the 2p orbital located in the central C atom promoted the binding of Li^+ and Ge^{4+} with the organic molecular structures. Moreover, Li^+ was observed to generate a significant bending of the aromatic structures in the A3 adsorption site (Figure 5a,c), while Ge^{4+} caused a slight bending of the aromatic structures (Figure 5b,d). The discrepancy in the degree of bending was due to the difference in the number of electrons transferred by the critical metal and the properties of the ions themselves.

3.4. Bond Length Analysis. The bond strength of chemical bonds between organic molecular structures and critical metals in coal can be studied using the Pauling correlation that bond order decreases as the bond length increases.[60] The average bond lengths between O−Li^+, C−Li^+, O−Ge^{4+}, and C−Ge^{4+} were statistically analyzed, as shown in Figure 6. The exact value of each bond is summarized in Table S2.

Obviously, on the surface of the organic molecular structures in coal, either Li^+ or Ge^{4+} was connected to oxygen functional groups and aromatic structures with various possible forms. In the organic molecular structures of lignite, the shortest distance between Li^+ and the oxygen functional group was 1.906 Å at the L4 adsorption site. This was the same as the binding site indicated by the ESP and HOMO. This was also the same as the Mulliken charge transfer trend. The longest distance between Li^+ and the oxygen functional groups was 2.132 Å at the L1 adsorption site. The bond lengths between Li^+ and aromatic structures changed slightly at the L5 to L8 adsorption sites, and the distances between them are all above 2.3 Å. In both bituminous and anthracite organic molecular structures, the distance between Li^+ and the oxygen functional groups was smaller than that between them and the aromatic structures (Figure 6a). The binding of Ge^{4+} to organic molecular structures showed the same trend. In the organic molecular structures of lignite, the shortest distance between Ge^{4+} and the oxygen functional groups was 1.954 Å at the L4 adsorption site. The

https://doi.org/10.1021/acsomega.3c01801
ACS Omega 2023, 8, 17264−17273

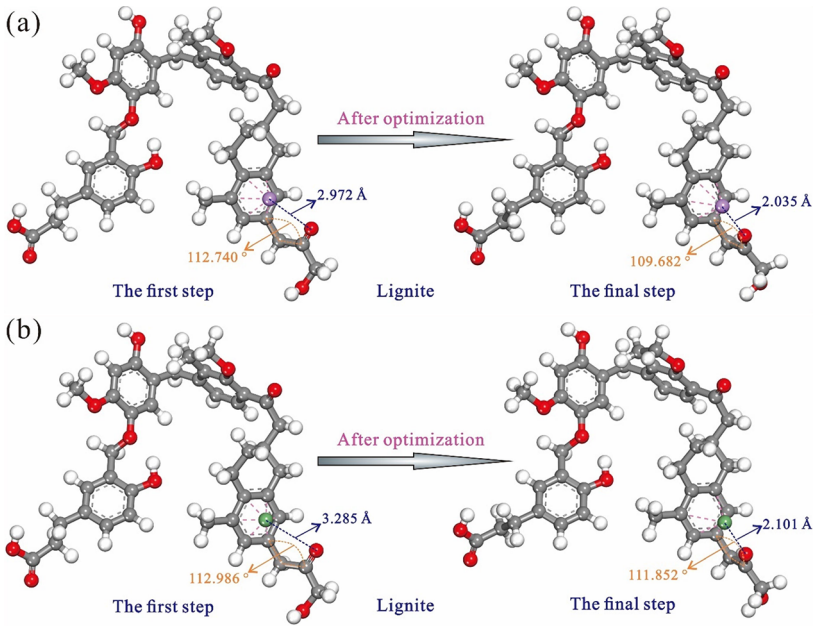

Figure 7. Changes in the spatial configuration of organic molecular structures after adsorption of critical metals. The distance between the critical metals and O51 is significantly shorter from the first step of adsorption to the final step of adsorption, and ∠C43C47C48 also considerably decreases. (a, b) Organic molecular structures of lignite.

distances between Ge^{4+} and aromatic structures were larger than 2.4 Å at L5 to L8 adsorption sites. In both bituminous and anthracite organic molecular structures, the distance between Ge^{4+} and the oxygen functional groups was smaller than that between them and the aromatic structures (Figure 6b). Therefore, the critical metals (Li^+ and Ge^{4+}) preferentially bind to the oxygen functional groups in the organic molecular structures. However, the binding strength must be analyzed comprehensively because of the synergistic interactions of oxygen-containing functional groups and aromatic structures for critical metals (Li^+ and Ge^{4+}). The O−Li^+/Ge^{4+} and C−Li^+/Ge^{4+} bond strength is not comparable to their bond length value because the ion radius of Li^+ and Ge^{4+} is different. The bond strength in this situation will be discussed in the following section.

3.5. MBO Analysis. The MBO explains the relative strength of bonds in a molecular structure.[61,62] The MBO accurately describes the bonds, numerically close to the real bond order, allowing the bond formation and breakage during the reaction to be visualized. A chemical bond is formed between two atoms when the MBO value is higher than 0.5.[63] If the MBO value is lower than 0.5, it is called a weak bond.[59] The exact value can be found in Table S3.

The MBO values of Li^+ bound with oxygen functional groups were less than 0.5. They did not form any MBO values with aromatic structures, indicating a weak binding ability of Li^+ with organic molecular structures in coal. In the organic molecular structures of lignite, the maximum MBO values of Li−O were located at L4 (0.2171) adsorption sites. This was the same as the binding site indicated by the ESP and HOMO. It was also found that L2, L3, and L4 adsorption sites all formed bidentate chelates, with average MBO values of their Li−O being 0.1533, 0.1650, and 0.1886, respectively. The bidentate structure was considered the strongest form of complexation, and mixed functional groups can effectively stabilize the metal complex.[32,33,36] Moreover, the L8 adsorption site was initially intended to study the binding ability of Li^+ with the aromatic structures, but carbonyl (O51) showed strong adsorption to Li^+, resulting in the formation of an MBO value of 0.1656 (O51−Li97) (Figure 7a), and Li^+ formed a 0.1665 MBO value with the carbonyl group (O10) at the L1 adsorption site. In the organic molecular structures of bituminous, the MBO values formed by B1 adsorption sites were 0.1028 (C4−Li33) and 0.1976 (O16−Li33), respectively. In the organic molecular structures of anthracite, the adsorption sites of A1 and A2 were both hydroxyl and symmetric, so their MBO values were almost the same, which were 0.1774 (O43−Li65) and 0.1746 (O45−Li65), respectively. It was not difficult to find that oxygen functional groups mainly controlled the binding of Li^+ with the organic molecular structures in coal, especially the presence of the carbonyl group (C═O). This was consistent with the finding that Li^+ tends to bind with oxygen to form stable complexes.[64] The Mulliken charge transfer and bond length analysis also proved that Li^+ preferred to be bound with oxygen.

The MBO values of Ge^{4+} bound with oxygen functional groups and aromatic structures indicated its strong binding ability with the organic molecular structure in coal. In the organic molecular structures of lignite, the maximum MBO value for Ge^{4+} bound with oxygen functional groups was at the L4 adsorption site, where the MBO value was 0.7839 (O52−Ge97). This was the same as the binding site indicated by the ESP and HOMO. Ge^{4+} formed strong MBO values of 0.6769, 0.5196, and 0.5520 at O10 (L1), O13 (L3), and O31 (L4) adsorption sites, respectively. The study found that the aromatic structure affected the binding of Ge^{4+} with oxygen functional groups at the L2 adsorption site. At the L2 adsorption site, the MBO values formed by O13 and O20 with Ge^{4+} were 0.4233 and 0.3620, respectively, and the MBO values formed by C1, C3, C5, and C6 with Ge^{4+} were 0.1140, 0.3069, 0.3773 and 0.1421, respectively. The influence of oxygen functional groups on the binding of Ge^{4+} with the aromatic structure was also observed. For example, at the L8 adsorption site, the original purpose was to study the interaction between Ge^{4+} and the aromatic structures, but carbonyl (O51) showed a strong adsorption

https://doi.org/10.1021/acsomega.3c01801
ACS Omega 2023, 8, 17264−17273

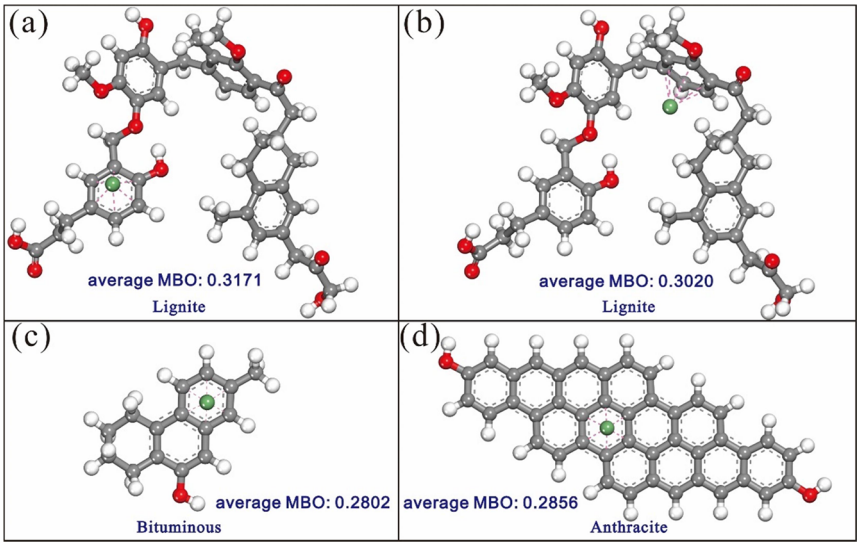

Figure 8. Average MBO values of half-sandwich complexes of Ge^{4+}−organic molecular structures. Organic molecular structures of (a, b) lignite, (c) bituminous, and (d) anthracite.

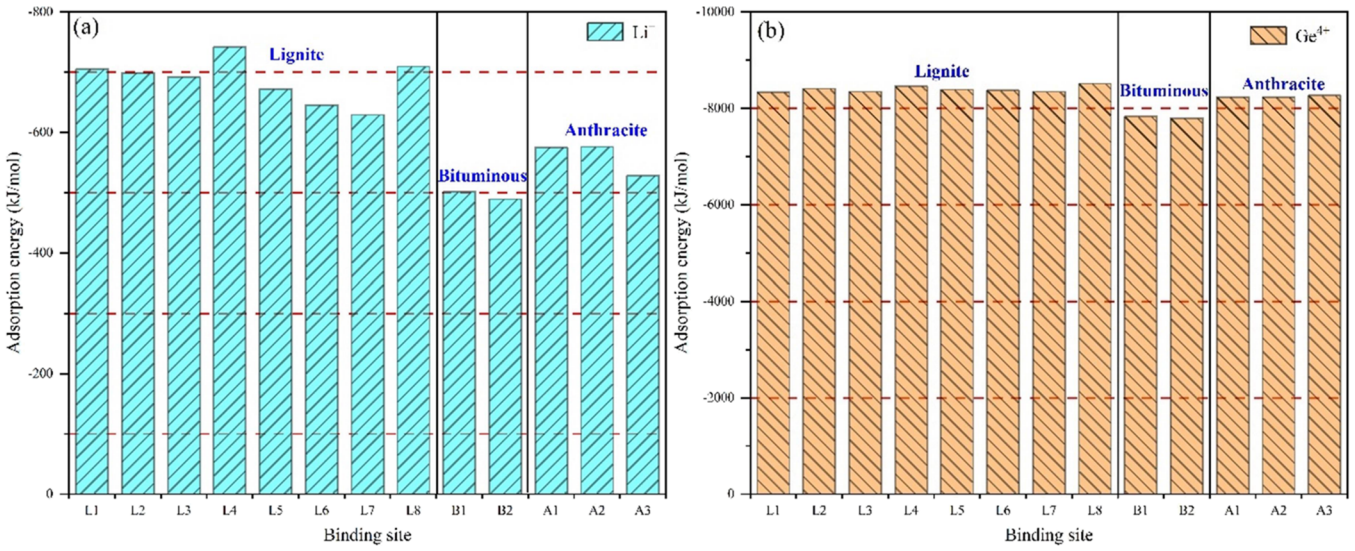

Figure 9. Adsorption energies (ΔE_{ads}) of different adsorption sites in organic molecular structures. (a) Li^+. (b) Ge^{4+}.

capacity to Ge^{4+}, forming an MBO value of 0.5020 (O51−Ge97) (Figure 7b). Additionally, two aromatic structures were found to interact with Ge^{4+} on the L6 adsorption site, including C14 (0.1435), C15 (0.4635), C16 (0.3768), C17 (0.2166), and C18 (0.1540) at the L6 adsorption site and C25 (0.1100) and C28 (0.4305) at the L7 adsorption site. This indicated a more complex bond of Ge^{4+} with organic molecular structures in coal. At the adsorption sites of L5 and L7, Ge^{4+} can interact with phenyl carbons to form stable half-sandwich complexes with aromatic structures (Figure 8a,b). Their average MBO values were 0.3171 and 0.3020, respectively. The complex of a half-sandwich is thermodynamically stable.[65] In the organic molecular structures of bituminous and anthracite, the MBO values of Ge^{4+} and the phenolic hydroxyl groups were more than 0.5, showing that Ge^{4+} can have a strong binding ability with the phenolic hydroxyl groups. This was the same as the results of the spectral analysis and DFT calculations by Wei et al.[28] Ge^{4+} also formed half-sandwich complexes at the B2 and A3 adsorption sites with average MBO values of 0.2802 and 0.2856, respectively (Figure 8c,d). It was slightly lower than the average MBO value formed by Ge^{4+} with the aromatic structure in the organic molecular structure of lignite. Therefore, the binding of Ge^{4+} with oxygen functional groups and aromatic structures in the organic molecular structure of coal all exhibited large adsorption ability.

3.6. Adsorption Energy Analysis. To further determine the stability of critical metals at different adsorption sites, adsorption energy calculations were performed. Figure 9 displays the findings of the adsorption energy calculation. The adsorption energies of Li^+ and Ge^{4+} at different adsorption sites were negative, indicating that the reaction was exothermic and spontaneous. For Li^+, in the organic molecular structures of lignite, the maximum adsorption energy of Li^+ bound with oxygen functional groups was at the L4 adsorption site, followed by L1, L2, and L3 adsorption sites. The adsorption energy values were −742.16, −705.00, −698.96, and −692.02 kJ/mol, respectively. Compared to aromatic structures, oxygen functional groups have higher adsorption energy for Li^+. Never-

https://doi.org/10.1021/acsomega.3c01801
ACS Omega 2023, 8, 17264−17273

theless, at the L8 adsorption site, the adsorption energy was as high as −709.49 kJ/mol. This was due to the influence of the carbonyl (O51) group. It is not difficult to find that carbonyl groups existed at the adsorption sites with large adsorption energy values. In particular, at the L8 adsorption site, the carbonyl group (O51) interaction led to a weak bond between Li^+ and the O51 atom. In the organic molecular structures of bituminous, the adsorption energy values of the B1 and B2 sites were −501.24 and −489.15 kJ/mol, respectively. The decrease in the adsorption energy value was due to the dramatic reduction in the carbonyl group in the organic molecular structure of lignite with the increase of the coal rank. The small molecular weight of the Wender bituminous model was also a non-negligible reason. Similarly, in the organic molecular structures of anthracite, the adsorption energy values of Li^+ bound with oxygen functional groups were more significant than those bound with aromatic structures (Figure 9a), indicating that the occurrence of Li^+ in coal was mainly affected by oxygen functional groups. This was consistent with the Mulliken charge, bond length, and MBO analysis results.

In contrast, there was no significant difference in the adsorption energy value of Ge^{4+} binding with oxygen functional groups and aromatic structures. In the organic molecular structures of lignite, the maximum adsorption energy of Ge^{4+} bound with oxygen functional groups was at the L4 adsorption site. This was followed by L2, L3, and L1 adsorption sites with adsorption energy values of −8461.85, −8407.79, −8345.20, and −8336.03 kJ/mol, respectively. The maximum adsorption energy of Ge^{4+} bound to the aromatic structures was at the L8 adsorption site. However, the L8 adsorption site was affected by the carbonyl group (O51), with an adsorption energy value of −8511.43 kJ/mol. At L5 and L7 adsorption sites, the adsorption energies of Ge^{4+} formed with aromatic structures were −8388.28 and −8345.65 kJ/mol, respectively, not significantly different from those formed by oxygen functional groups. In the organic molecular structures of bituminous and anthracite, the adsorption energy values of Ge^{4+} bound with oxygen functional groups and aromatic structures were almost the same (Figure 9b). The low adsorption energy value of the organic molecular structures of Wender bituminous cannot be excluded due to the small molecular weight. It was not difficult to find that the binding of Ge^{4+} with the organic molecular structure was less affected by the change of the coal rank, and Ge^{4+} showed strong binding ability for both oxygen functional groups and aromatic structures. This was the same result as the MBO analysis. The adsorption energy value of Ge^{4+} at the L8 adsorption site was highest due to the synergistic interactions of the oxygen functional groups and the aromatic structures. Therefore, the binding ability of the organic molecular structure with Ge^{4+} was enhanced by the synergistic interactions of oxygen functional groups and aromatic structures.

4. CONCLUSIONS

The modes of occurrence of critical metals in the organic molecular structures of coal are essential in determining its economic extraction potential. Accordingly, complete organic molecular structures will be selected to investigate further the relationship between critical metals and organic molecular structures in coal. The oxygen functional group interactions and π-cation interactions in organic molecular structures were studied in this paper using the representative Wender coal organic molecular structures. The main conclusions were as follows:

(1) The negative ESP, HOMO, and negative Mulliken charge analysis showed that both oxygen functional groups and aromatic structures in the organic molecular structure of coal can serve as critical metal-binding sites. Among them, the carbonyl group (C═O) in oxygen functional groups had the most significant influence on the occurrence of Li^+ in organic molecular structures. The strongest binding of organic molecular structures with Li^+ occurred at the L4 adsorption site. The adsorption energy value was −742.16 kJ/mol. In contrast, the binding of Li^+ with the aromatic structures was weak.

(2) The Mulliken charge, bond length, MBO, and adsorption energy data analyses showed that the binding of Ge^{4+} with organic molecular structures was more complex. The binding of Ge^{4+} with oxygen functional groups and aromatic structures in the organic molecular structure of coal all exhibited large adsorption energy values. Therefore, the coal rank had little effect on the binding of Ge^{4+} with organic molecular structures. In addition, the binding ability of the organic molecular structure with Ge^{4+} was enhanced by the synergistic interactions of oxygen functional groups and aromatic structures. The organic molecular structure and Ge^{4+} had the largest adsorption energy value at the L8 adsorption site of −8511.43 kJ/mol.

(3) The changes in the spatial configuration of organic molecular structures were caused by the adsorption of organic matter in coal to critical metals. For example, the adsorption of carbonyl groups (O51) to Li^+ and Ge^{4+} resulted in local twisting of the organic molecular structure of lignite. In contrast, the adsorption of anthracite organic molecular structures to Li^+ and Ge^{4+} resulted in the bending of the aromatic structures. In particular, Li^+ caused a more obvious bending of the aromatic structure.

■ ASSOCIATED CONTENT

Supporting Information

The Supporting Information is available free of charge at https://pubs.acs.org/doi/10.1021/acsomega.3c01801.

Mulliken charges transfer of critical metals at different adsorption sites (Table S1); average bond length values between critical metals and organic molecular structures (Table S2); and MBO values of critical metals at different adsorption sites (Table S2) (PDF)

■ AUTHOR INFORMATION

Corresponding Author

Shaoqing Wang − *College of Geoscience and Surveying Engineering, China University of Mining and Technology (Beijing), Beijing 100083, China;* orcid.org/0000-0001-5158-7751; Email: wangzq@cumtb.edu.cn

Authors

Ruifeng Mu − *College of Geoscience and Surveying Engineering, China University of Mining and Technology (Beijing), Beijing 100083, China*

Xiaoling Wang − *College of Geoscience and Surveying Engineering, China University of Mining and Technology (Beijing), Beijing 100083, China*

https://doi.org/10.1021/acsomega.3c01801
ACS Omega 2023, 8, 17264−17273

Yungang Zhao − *College of Geoscience and Surveying Engineering, China University of Mining and Technology (Beijing), Beijing 100083, China*

Zeyu Dong − *College of Geoscience and Surveying Engineering, China University of Mining and Technology (Beijing), Beijing 100083, China*

Complete contact information is available at: https://pubs.acs.org/10.1021/acsomega.3c01801

Notes

The authors declare no competing financial interest.

■ ACKNOWLEDGMENTS

We gratefully thank the National Key Research and Development Program of China (Research Project No. 2021YFC2902000) and the National Natural Science Foundation of China (Research Project No. 42030807) for their financial support.

■ REFERENCES

(1) Tkaczyk, A. H.; Bartl, A. L.; Amato, A.; Lapkovskis, V.; Petranikova, M. Sustainability evaluation of essential critical raw materials: cobalt, niobium, tungsten and rare earth elements. *J. Phys. D: Appl. Phys.* **2018**, *51*, 203001.

(2) Seredin, V. V.; Finkelman, R. B. Metalliferous coals: A review of the main genetic and geochemical types. *Int. J. Coal Geol.* **2008**, *76*, 253−289.

(3) Sun, Y. Z. China geological survey proved the existence of an extra-large coal-associated lithium deposit. *Acta Geol. Sin.* **2015**, *89*, 311.

(4) Qin, S. J.; Sun, Y. Z.; Li, Y. H.; Wang, J. X.; Zhao, C. L.; Gao, K. Coal deposits as promising alternative sources for gallium. *Earth-Sci. Rev.* **2015**, *150*, 95−101.

(5) Qin, S. J.; Zhao, C. L.; Li, Y. H.; Zhang, Y. Review of coal as a promising source of lithium. *Int. J. Oil, Gas Coal Technol.* **2015**, *9*, 215−229.

(6) Dai, S. F.; Finkelman, R. B. Coal as a promising source of critical elements: Progress and future prospects. *Int. J. Coal Geol.* **2018**, *186*, 155−164.

(7) Sun, Y. Z.; Zhao, C. L.; Li, Y. H.; Wang, J. X.; Zhang, J. Y.; Jin, Z.; Lin, M. Y.; Wolfgang, K. Further information of the associated li deposits in the No.6 coal seam at Jungar coalfield, Inner Mongolia, Northern China. *Acta Geol. Sin.* **2013**, *87*, 1097−1108.

(8) Dai, S. F.; Yan, X. Y.; Ward, C. R.; Hower, J. C.; Zhao, L.; Wang, X. B.; Zhao, L. X.; Ren, D. Y.; Finkelman, R. B. Valuable elements in Chinese coals: a review. *Int. Geol. Rev.* **2018**, *60*, 590−620.

(9) Dai, S. F.; Zhao, L.; Wei, Q.; Song, X. L.; Wang, W. F.; Liu, J. J.; Duan, P. P. Resources of critical metals in coal-bearing sequences in China: Enrichment types and distribution. *Chin. Sci. Bull.* **2020**, *65*, 3715−3729.

(10) Seredin, V. V.; Dai, S. F.; Sun, Y. Z.; Chekryzhov, I. Y. Coal deposits as promising sources of rare metals for alternative power and energy-efficient technologies. *Appl. Geochem.* **2013**, *31*, 1−11.

(11) Dai, S. F.; Seredin, V. V.; Ward, C. R.; Jiang, J. H.; Hower, J. C.; Song, X. L.; Jiang, Y. F.; Wang, X. B.; Gornostaeva, T.; Li, X.; Liu, H. D.; Zhao, L. X.; Zhao, C. L. Composition and modes of occurrence of minerals and elements in coal combustion products derived from high-Ge coals. *Int. J. Coal Geol.* **2014**, *121*, 79−97.

(12) Dai, S. F.; Liu, C. Y.; Zhao, L.; Liu, J. J.; Wang, X. B.; Ren, D. Y. Strategic metal resources in coal-bearing strata: significance and challenges. *J. China Coal Soc.* **2022**, *47*, 1743−1749, DOI: 10.13225/j.cnki.jccs.MJ22.0011.

(13) Qin, S. J.; Lu, Q. F.; Li, Y. H.; Wang, J. X.; Zhao, Q. J.; Gao, K. Relationships between trace elements and organic matter in coals. *J. Geochem. Explor.* **2018**, *188*, 101−110.

(14) Lewińska-Preis, L.; Fabiańska, M. J.; Ćmiel, S.; Kita, A. Geochemical distribution of trace elements in Kaffioyra and Longyearbyen coals, Spitsbergen, Norway. *Int. J. Coal Geol.* **2009**, *80*, 211−223.

(15) Liang, H. Z.; Zeng, F. G.; Xiang, J. H.; Li, M. F. Geochemical characteristics and inorganic-organic affinity of the trace elements in Yimin lignite. *J. Fuel Chem. Technol.* **2013**, *41*, 1173−1183. (in Chinese with English abstract)

(16) Rajabzadeh, M. A.; Ghorbani, Z.; Keshavarzi, B. Chemistry, mineralogy and distribution of selected trace-elements in the Parvadeh coals, Tabas, Iran. *Fuel* **2016**, *174*, 216−224.

(17) Finkelman, R. B.; Palmer, C. A.; Wang, P. Quantification of the modes of occurrence of 42 elements in coal. *Int. J. Coal Geol.* **2018**, *185*, 138−160.

(18) Dai, S. F.; Finkelman, R. B.; French, D.; Hower, J. C.; Graham, I. T.; Zhao, F. H. Modes of occurrence of elements in coal: A critical evaluation. *Earth-Sci. Rev.* **2021**, *222*, No. 103815.

(19) Shpirt, M. Y.; Kler, V. R.; Pertcikov, I. Z. Inorganic Components of Solid Fuels. *Khimija: Moscow* **1990**, 240.

(20) Dai, S. F.; Wang, X. B.; Seredin, V. V.; Hower, J. C.; Ward, C. R.; O'Keefe, J. M. K.; Huang, W. H.; Li, T.; Li, X.; Liu, H. D.; Xue, W. F.; Zhao, L. X. Petrology, mineralogy, and geochemistry of the Ge-rich coal from the Wulantuga Ge ore deposit, Inner Mongolia, China: New data and genetic implications. *Int. J. Coal Geol.* **2012**, *90−91*, 72−99.

(21) Dai, S. F.; Liu, J. J.; Ward, C.; Hower, J.; Xie, P. P.; Jiang, Y. F.; Hood, M.; O'Keefe, J.; Song, H. J. Petrological, geochemical, and mineralogical compositions of the low-Ge coals from the Shengli Coalfield, China: A comparative study with Ge-rich coals and a formation model for coal-hosted Ge ore deposit. *Ore Geol. Rev.* **2015**, *71*, 318−349.

(22) Dai, S. F.; Wang, P. P.; Ward, C. R.; Tang, Y. G.; Song, X. L.; Jiang, J. H.; Hower, J. C.; Li, T.; Seredin, V. V.; Wagner, N. J.; Jiang, Y. F.; Wang, X. B.; Liu, J. J. Elemental and mineralogical anomalies in the coal-hosted Ge ore deposit of Lincang, Yunnan, southwestern China: Key role of N_2−CO_2-mixed hydrothermal solutions. *Int. J. Coal Geol.* **2015**, *152*, 19−46.

(23) Etschmann, B.; Liu, W. H.; Li, K.; Dai, S. F.; Reith, F.; Falconer, D.; Kerr, G.; Paterson, D.; Howard, D.; Kappen, P.; Wykes, J.; Brugger, J. Enrichment of germanium and associated arsenic and tungsten in coal and roll-front uranium deposits. *Chem. Geol.* **2017**, *463*, 29−49.

(24) Manskaya, S. M.; Kodina, L. A.; Generalova, V. N.; Kravtsova, R. P. Interaction between Ge and lignin structures in the early stages of formation of coal. *Geochem. Int.* **1972**, *9*, 385−394.

(25) Zhuang, H. P.; Lu, J. L.; Fu, J. M.; Liu, J. Z. Lincang Superlarge Germanium Deposit in Yunnan Province, China: Sedimentation, Diagenesis, Hydrothermal Process and Mineralization. *J. China Univ. Geosci.* **1998**, *9*, 129−136.

(26) Pokrovski, G. S.; Schott, J. Experimental study of the complexation of silicon and germanium with aqueous organic species: implications for germanium and silicon transport and Ge/Si ratio in natural waters. *Geochim. Cosmochim. Acta* **1998**, *62*, 3413−3428.

(27) Pokrovski, G. S.; Martin, F.; Hazemann, J.-L.; Schott, J. An X-ray absorption fine structure spectroscopy study of germanium-organic ligand complexes in aqueous solution. *Chem. Geol.* **2000**, *163*, 151−165.

(28) Wei, Q.; Cui, C. N.; Dai, S. F. Organic-association of Ge in the coal-hosted ore deposits: An experimental and theoretical approach. *Ore Geol. Rev.* **2020**, *117*, No. 103291.

(29) Dougherty, D. A. Interactions in Chemistry and Biology: A New View of Benzene, Phe, Tyr, and Trp. *Science* **1996**, *271*, 163−168.

(30) Lemli, B.; Kánnár, D.; Nie, J. C.; Li, H. J.; Kunsági-Máté, S. Some Unexpected Behavior of the Adsorption of Alkali Metal Ions onto the Graphene Surface under the Effect of External Electric Field. *J. Phys. Chem. C* **2013**, *117*, 21509−21515.

(31) Opaprakasit, P.; Scaroni, A. W.; Painter, P. C. Ionomer-Like Structures and π-Cation Interactions in Argonne Premium Coals. *Energy Fuels* **2002**, *16*, 543−551.

(32) He, H. T.; Xing, L. C.; Zhang, J. S.; Tang, M. Binding characteristics of Cd^{2+}, Zn^{2+}, Cu^{2+}, and Li^{+} with humic substances: Implication to trace element enrichment in low-rank coals. *Energy Explor. Exploit.* **2016**, *34*, 735−745.

(33) Xing, L. C.; He, H. T.; Xu, B. H.; Zhang, J. S.; Yan, Z. F.; Jin, C.; Li, J.; Liu, L. T. Rethinking enrichments of trace element in low-rank coals: Preliminarily quantifying the effectiveness of local structure to stabilize humates. *Energy Explor. Exploit.* **2018**, *36*, 1645−1654.
(34) Zhang, Z. J.; Zhou, Q.; Zhuang, L.; Zhao, Z. Y. Adsorption of Ca(II) and K(I) on the kaolinite surface: a DFT study with an experimental verification. *Mol. Phys.* **2021**, *119*, No. 1896047.
(35) Zhang, K.; Li, H. L.; Li, Z. G.; Qi, S.; Cui, S. Y.; Chen, W. Z.; Wang, S. Q. Molecular dynamics and density functional theory simulations of cesium and strontium adsorption on illite/ smectite. *J. Radioanal. Nucl. Chem.* **2022**, *331*, 2983−2992.
(36) Sundararajan, M.; Rajaraman, G.; Ghosh, S. K. Speciation of uranyl ions in fulvic acid and humic acid: a DFT exploration. *Phys. Chem. Chem. Phys.* **2011**, *13*, 18038−18046.
(37) Kim, K. H.; Jeong, K.; Kimc, S. S.; Brown, R. C. Kinetic understanding of the effect of Na and Mg on pyrolytic behavior of lignin using a distributed activation energy model and density functional theory modeling. *Green Chem.* **2019**, *21*, 1099−1107.
(38) Jeong, K.; Jeong, H. J.; Lee, G.; Kim, S. H.; Kim, K. H.; Yoo, C. G. Catalytic Effect of Alkali and Alkaline Earth Metals in Lignin Pyrolysis: A Density Functional Theory Study. *Energy Fuels* **2020**, *34*, 9734−9740.
(39) Sun, Y. Z.; Zhao, C. L.; Qin, S. J.; Xiao, L.; Li, Z. S.; Lin, M. Y. Occurrence of some valuable elements in the unique 'high-aluminium coals' from the Jungar coalfield, China. *Ore Geol. Rev.* **2016**, *72*, 659−668.
(40) Wender, I. Catalytic Synthesis of Chemicals from Coal. *Catal. Rev.* **1976**, *14*, 97−129.
(41) Zhou, Z. J.; Guo, L.; Chen, L. P.; Shan, S. Q.; Wang, Z. H. Study of pyrolysis of brown coal and gasification of coal-water slurry using the ReaxFF reactive force field. *Int. J. Energy Res.* **2018**, *42*, 2465−2480.
(42) Li, B.; Liu, S. Y.; Fan, M. Q.; Zhang, L. Interfacial water at the low-rank coal surface: an experiment and simulation study. *Theor. Chem. Acc.* **2018**, *137*, 1−9.
(43) Yang, Y. J.; Liu, J. J.; Wang, Z. Reaction mechanisms and chemical kinetics of mercury transformation during coal combustion. *Prog. Energy Combust. Sci.* **2020**, *79*, No. 100844.
(44) Yang, Y. H.; Pan, J. N.; Hou, Q. L.; Wang, K.; Wang, X. L. Stress degradation mechanism of coal macromolecular structure: Insights from molecular dynamics simulation and quantum chemistry calculations. *Fuel* **2021**, *303*, No. 121258.
(45) Jin, H.; Zhang, Y. S.; Dong, H. T.; Zhang, Y. N.; Sun, Y. J.; Shi, J.; Li, R. T. Molecular dynamics simulations and experimental study of the effects of an ionic surfactant on the wettability of low-rank coal. *Fuel* **2022**, *320*, No. 123951.
(46) Schobert, H. H. *The Chemistry of Hydrocarbon Fuels*; Butterworth: London, 1990; Vol. *123*.
(47) Erdenetsogt, B. O.; Lee, I.; Lee, S. K.; Ko, Y. J.; Bat-Erdene, D. Solid-state C-13 CP/MAS NMR study of Baganuur coal, Mongolia: Oxygen-loss during coalification from lignite to subbituminous rank. *Int. J. Coal Geol.* **2010**, *82*, 37−44.
(48) Liu, Y.; Liu, W. B.; Wang, R. G.; Hao, L. F.; Jiao, W. C. Hydrogen storage using Na-decorated graphyne and its boron nitride analog. *Int. J. Hydrogen Energy* **2014**, *39*, 12757−12764.
(49) Ayub, K. Are phosphide nano-cages better than nitride nano-cages? A kinetic, thermodynamic and non-linear optical properties study of alkali metal encapsulated X12Y12 nano-cages. *J. Mater. Chem. C* **2016**, *4*, 10919−10934.
(50) Perdew, J. P.; Burke, K.; Ernzerhof, M. Generalized Gradient Approximation Made Simple. *Phys. Rev. Lett.* **1996**, *77*, 3865−3868.
(51) Grimme, S. Semiempirical GGA-type density functional constructed with a long-range dispersion correction. *J. Comput. Chem.* **2006**, *27*, 1787−1799.
(52) Yu, H. J.; Zheng, L. C.; Zhang, T.; Ren, J. J.; Cheng, W.; Zhang, L. J.; Meng, P. P. Adsorption behavior of Cd (II) on TEMPO-oxidized cellulose in inorganic/ organic complex systems. *Environ. Res.* **2021**, *195*, No. 110848.
(53) Zhao, Y. G.; Wang, S. Q.; Liu, Y.; Song, X. X.; Chen, H.; Zhang, X. M.; Lin, Y. H.; Wang, X. L. Molecular Modeling and Reactivity of Thermally Altered Coals by Molecular Simulation Techniques. *Energy Fuels* **2021**, *35*, 15663−15674.
(54) Li, X. D.; Tang, Y. J.; Wang, C. Y.; Zhang, H.; Cheng, X. L. A DFT Investigation on Hydrogen Adsorption Based on Alkali-metal Organic Complexes. *Chin. J. Struct. Chem.* **2010**, *29*, 1404−1410.
(55) Al-Azawi, K. F.; Al-Baghdadi, S. B.; Mohamed, A. Z.; Al-Amiery, A. A.; Abed, T. K.; Mohammed, S. A.; Kadhum, A. A. H.; Mohamad, A. B. Synthesis, inhibition effects and quantum chemical studies of a novel coumarin derivative on the corrosion of mild steel in a hydrochloric acid solution. *Chem. Cent. J.* **2016**, *10*, 23.
(56) Thul, P.; Gupta, V. P.; Ram, V. J.; Tandon, P. Structural and spectroscopic studies on 2-pyranones. *Spectrochim. Acta, Part A* **2010**, *75*, 251−260.
(57) Pan, S.; Wang, Q.; Bai, J. R.; Chi, M. S.; Cui, D.; Wang, Z. C.; Liu, Q.; Xu, F. Molecular Structure and Electronic Properties of Oil Shale Kerogen: An Experimental and Molecular Modeling Study. *Energy Fuels* **2018**, *32*, 12394−12404.
(58) Li, K.; Li, N.; Yan, N. N.; Wang, T. Y.; Zhang, Y. T.; Song, Q.; Li, H. J. Adsorption of small hydrocarbons on pristine, N-doped and vacancy graphene by DFT study. *Appl. Surf. Sci.* **2020**, *515*, No. 146028.
(59) Liu, Z. G.; Chen, T.; Hu, C. H.; Wang, D. H.; Wang, Z. M.; Li, G. Y. Calculation and analysis of interaction between characteristic functional group of persimmon tannin and metal ions. *Acta Phys. Sin.* **2021**, *70*, No. 123101.
(60) Amaldi, E.; Pauling, L. The Nature of the Chemical Bond. *Scientia* **1947**, *41*, 78.
(61) Mayer, I. Charge, bond order and valence in the AB initio SCF theory. *Chem. Phys. Lett.* **1983**, *97*, 270−274.
(62) Alhameedi, K.; Karton, A.; Jayatilaka, D.; Thomas, S. P. Bond orders for intermolecular interactions in crystals: charge transfer, ionicity and the effect on intramolecular bonds. *IUCrJ* **2018**, *5*, 635−646.
(63) Mayer, I. Bond order and valence indices: a personal account. *J. Comput. Chem.* **2007**, *28*, 204−221.
(64) Nieboer, E.; Richardson, D. H. S. The replacement of the nondescript term 'heavy metals' by a biologically and chemically significant classification of metal ions. *Environ. Pollut., Ser. B* **1980**, *1*, 3−26.
(65) Severin, K. Supramolecular chemistry with organometallic half-sandwich complexes. *Chem. Commun.* **2006**, 3859−3867.

https://doi.org/10.1021/acsomega.3c01801
ACS Omega 2023, 8, 17264−17273